SLAC–PUB–7969
December 1998

Final Focus Systems in Linear Colliders*

T.O. Raubenheimer and F. Zimmermann

Stanford Linear Accelerator Center
Stanford University, Stanford, CA 94309, USA

In colliding beam facilities, the "final focus system" must demagnify the beams to attain the very small spot sizes required at the interaction points. The first final focus system with local chromatic correction was developed for the Stanford Linear Collider where very large demagnifications were desired. This same conceptual design has been adopted by all the future linear collider designs as well as the SuperConducting Supercollider, the Stanford and KEK B-Factories, and the proposed Muon Collider. In this paper, the overall layout, physics constraints, and optimization techniques relevant to the design of final-focus systems for high-energy electron-positron linear colliders are reviewed. Finally, advanced concepts to avoid some of the limitations of these systems are discussed.

Submitted to
Reviews of Modern Physics

*Work supported by the Department of Energy under the contract DE–AC03–76SF00515.

Final Focus Systems in Linear Colliders*

T.O. Raubenheimer and F. Zimmermann

Stanford Linear Accelerator Center

Stanford University

P.O.Box 4349

Stanford, CA 94309

U.S.A.

Abstract

In colliding beam facilities, the "final focus system" must demagnify the beams to attain the very small spot sizes required at the interaction points. The first final focus system with local chromatic correction was developed for the Stanford Linear Collider where very large demagnifications were desired. This same conceptual design has been adopted by all the future linear collider designs as well as the SuperConducting Supercollider, the Stanford and KEK B-Factories, and the proposed Muon Collider. In this paper, the overall layout, physics constraints, and optimization techniques relevant to the design of final-focus systems for high-energy electron-positron linear colliders are reviewed. Finally, advanced concepts to avoid some of the limitations of these systems are discussed.

---

*Work supported by the Department of Energy under the contract DE-AC03-76SF00515.

Contents

I. INTRODUCTION

Particle physics is an experimental science studying the fundamental forces and elementary particles which form the building blocks of our natural world. Most of the processes of interest become apparent at high energies. For this reason, most progress in our understanding of nature, from the atomic structure to the quarks and gluons inside a proton, has been made by colliding high-energy particles, usually protons and antiprotons, or electrons and positrons. For the past few decades, these particles were accelerated and collided in circular storage rings, the sole exception being the Stanford Linear Collider (SLC) (Seeman, 1990). In a storage ring, synchrotron radiation emitted by the bent electrons causes an energy loss per turn that, for constant bending radius, increases with the fourth power of the beam energy. Because this radiated energy must be replaced with a costly rf system, the radiation effectively limits the maximum energy of circular e^+/e^- storage rings. The largest circular collider ever built is the LEP ring in Geneva (Myers, 1995) which has a 30 km circumference with a beam energy close to 100 GeV.

It is generally assumed (Loew, 1995) that the generation of electron-positron colliders following LEP must be linear colliders, with the SLC as a successful prototype. In a linear collider, the beams are accelerated in straight linear accelerators aimed at the collision point to reduce the synchrotron radiation problems. Instead of having the optimized cost increase as the energy squared, the cost of the linear collider is roughly proportional to the final energy. As an example of a future linear collider design, a schematic of the Stanford Next Linear Collider (NLC) design is illustrated in Figure 1. The linear collider complex consists of two roughly equivalent halves which are aimed at each other. Each half is composed of an injector complex for beam generation, a damping ring which improves the beam quality, a linear accelerator in which the beam gains the desired energy, a collimation system which removes the beam halo that otherwise could cause background in the particle-physics detector, a final focus system, and the collision point, followed on the other side by an exit line for the spent beam.

Although linear colliders avoid the limitation due to synchrotron radiation in a storage ring, there are other problems, namely, accelerating the beams and producing the very small spot sizes that are necessary at the interaction point (IP). The small spot sizes are necessary to achieve reasonable reaction rates. This arises because the reaction rate is given by the process cross-section, which tends to decrease with the square of the center-of-mass energy, multiplied by the collider luminosity. Assuming gaussian beams and head-on collisions, the collider luminosity can be written:

$$\mathcal{L} \approx \frac{f_{rep}}{2\pi} \frac{n_b N_+ N_-}{\Sigma_x \Sigma_y} \tag{1}$$

where f_{rep} is the collider repetition rate, n_b, and $N_\pm$ are the number of bunches per pulse and the charge per bunch, and $\Sigma_{x,y}$ are the sum in quadrature of the horizontal and vertical sizes of the colliding beams.

Unlike a storage ring, the high-energy beams in a linear collider are only collided once, and must be regenerated each pulse. In view of technological limits on the linear-accelerator repetition rate, and in order to constrain the power consumption of the collider, the collision frequency f_{rep} is two or three orders of magnitude smaller than in a storage ring. Thus, to attain comparable luminosity, the linear colliders accelerate long trains of bunches and focus them to very small spot sizes. Fortunately, because the beams are not collided again the minimum spot size is not limited by the beam-beam tune shift as it is in a circular collider. However, the small spot sizes impose severe requirements on the final focus system of the linear collider. For example, in the next-generation of linear colliders, the collision spot size is measured in nanometers; parameters of a few circular and linear colliders are compared in Table I.

The purpose of the final focus system (FFS) in a linear collider is to demagnify the beams to the very small spot sizes required at the IP. In principle, the FFS operates as a simple telescope. However, the strong focusing quadrupoles that produce the small spots also generate very large chromaticities. Thus, to focus a beam with a finite energy spread, the system must be chromatically corrected. The normal procedure is to perform the chromatic correction by

	Luminosity	f_{rep}	n_b	$N[10^{10}]$	$\sigma_x\,[\mu\mathrm{m}]$	$\sigma_y\,[\mu\mathrm{m}]$
NLC	1×10^{34}	120 Hz	90	1	0.25	0.004
SLC	2×10^{30}	120 Hz	1	4	1.5	0.5
PEP-II	3×10^{33}	140 kHz	1700	4	155	6
LEP2	5×10^{31}	10 kHz	8	30	240	4

placing sextupole magnets in regions of dispersion where pairs of sextupoles are separated by 180° in betatron phase (a $-I$ transformation) so that the geometric aberrations cancel. However, the sextupoles introduce higher-order geometric and chromo-geometric aberrations which may have to be controlled with careful placement of the elements or additional multipole magnets. It should be noted that similar chromatic cancellation techniques for the final focus had been adopted for the SuperConducting Supercollider, the Stanford and KEK B-Factories, and the proposed Muon Collider.

In most linear collider designs, the IP spots are asymmetric: the vertical spot size is much smaller than the horizontal; this maximizes the luminosity while minimizing the beam-beam interaction and easing the constraints on the final focus. Typical designs have a demagnification of a few hundred in the vertical plane with an order-of-magnitude less in the horizontal. The vertical focusing is usually set close to the limit from the depth of focus, i.e. $\beta_y \sim \sigma_z$, but other constraints, such as the chromaticity or tolerances on the components, may lead to a weaker optimal choice. In the following, we will describe the basic layout of a final focus system and then discuss many of the limitations which must be considered in the design. Finally, we will describe some of the design and optimization techniques that are important and some of the more advanced concepts that have been proposed. Throughout this article, we will ignore many of the more design specific issues such as detailed tolerance calculations, collimation, masking, and machine protection. Detailed discussions of all the relevant effects can be found in any of the future linear collider design documents (Zeroth Order Design Report, 1996; JLC Design Study, 1997; DESY Linear Collider Design Report,

1997) or in Ref. (Roy, 1992), which discusses the FFTB design, and many of the detailed expressions used in this note originate in Refs. (Zeroth Order Design Report, 1996; Roy, 1992).

II. LAYOUT

The first linear collider FFS in operation is that at the Stanford Linear Collider (SLC) (Brown and Spencer, 1981; Murray *et al.*, 1987). To save space, the SLC final focus was designed with an interleaved horizontal and vertical chromatic correction section. Unfortunately, the interleaved sextupoles introduce higher-order aberrations. While these aberrations are not a severe limitation in the SLC, they would be in systems with greater demagnification.

To limit the high-order aberrations, most of the next-generation FFS have been designed in a modular manner with separate sections for horizontal and vertical chromaticity correction. Thus, a typical final focus system consists of a beta matching section to adjust the final focus for the incoming beam, a diagnostic region to verify the incoming beam properties, a horizontal chromaticity correction section (CCX), a beta exchange region (BX), a vertical chromaticity correction section (CCY), a final transformer (FT), and the final lens which is usually a quadrupole doublet (FD). Figure 2 illustrates the optics in the Final Focus Test Beam FFTB at Stanford (FFTB Design Report, 1991) which is a model for the final focus in a future linear collider.

Most next-generation linear collider designs operate with long trains of bunches to make more efficient use of the rf systems. When these bunches are closely spaced, the FFS are designed with beam trajectories intersecting at a "crossing angle" Θ_c at the IP. This avoids any parasitic bunch collisions and provides a method of separating the incoming and outgoing beams so that the later can be directed to the beam dumps. Unfortunately, this crossing angle will reduce the luminosity unless the beams are "crabbed", i.e. tilted in x-z space so that they pass through each other head-on.

III. LUMINOSITY

The luminosity in a linear collider can be expressed as (Chen and Yokoya, 1992)

$$\mathcal{L} = \mathcal{L}_0 \tilde{H}_D = \mathcal{L}_{00} H_D \ . \tag{2}$$

Here, H_D or $\tilde{H}_D$ characterizes the luminosity enhancement which depends upon the beam-beam interaction and is discussed in Section IV, $\mathcal{L}_{00}$ is the ideal luminosity for head-on collision and zero bunch length, $\mathcal{L}_0$ is the geometric luminosity including the effect of a finite bunch length and the depth of focus. The luminosity $\mathcal{L}_0$ depends on the beam properties as well as the FFS properties such as the depth of focus and the (horizontal) *bunch* crossing angle θ_c; note that with perfect crab crossing $\theta_c = 0$ while without crab crossing $\theta_c = \Theta_c$, the angle at which the trajectories cross.

The ideal short-bunch luminosity is

$$\mathcal{L}_{00} = \frac{f_{rep} n_b N_b^2}{4\pi \sigma_x^\star \sigma_y^\star} \tag{3}$$

and the actual geometric luminosity can be expressed as

$$\mathcal{L}_0 = \mathcal{L}_{00} \eta(C_\theta, A_y) \tag{4}$$

where f_{rep}, n_b, and N are the repetition rate, the number of bunches per pulse, and the bunch charge. In addition, $\sigma_{x,y}^\star$ are the rms beam sizes at the IP and η describes the effects due to depth of focus and the crossing angle. Assuming flat gaussian beams ($\sigma_x \gg \sigma_y$), η can be written

$$\eta(C_\theta, A_y) = \frac{1}{A_y \sqrt{\pi}} e^x K_0(x) \qquad\qquad x \equiv \frac{1 + C_\theta^2/4}{2A_y^2} \tag{5}$$

where K_0 is the modified Bessel function, $A_y \equiv \sigma_z / \beta_y^\star$ describes the depth of focus, and $C_\theta \equiv \theta_c \sigma_z / \sigma_x$ is the ratio of the bunch diagonal angle to the bunch crossing angle θ_c. The geometric luminosity loss is about 14% when $A_y = 1$ and is another 10% when $C_\theta = 1$. Typically, FFS are designed with $A_y \lesssim 1$ and $C_\theta \lesssim 1$. Techniques have been developed or proposed in order to reduce the sensitivity to the crossing angle, namely crab crossing which

is discussed in section V, and to the depth of focus, namely a 'traveling focus' which will be discussed in Section XIII.

IV. BEAM-BEAM INTERACTION

Excellent reviews of the beam-beam effects in linear colliders are available (Chen and Yokoya, 1988a; Chen and Yokoya, 1992). In the following we summarize some of the main features.

The collision strength at a linear collider is measured in terms of the horizontal and vertical disruption parameters

$$D_{x,y} = \frac{2N_b r_e \sigma_z}{\gamma \sigma^\star_{x,y}(\sigma^\star_x + \sigma^\star_y)} \tag{6}$$

where N_b denotes the number of particles per bunch and γ the relativistic Lorentz factor. In linear approximation, the number of oscillations a particle undergoes in the field of the opposing beam is $\sim \sqrt{\sqrt{3}D_{x,y}}/(2\pi)$. The parameter D is the equivalent of the beam-beam tune shift parameter in a ring collider (the two quantities are identical in the case $\beta^\star \approx \sigma_z$). Values for D can vary between 1 (SLC) and almost 10 (NLC).

During the collision, particles emit synchrotron radiation in the field of the opposing beam. This radiation is called beamstrahlung, and it is characterized by the Υ parameter, which is proportional to the average critical energy,

$$\Upsilon = \frac{2\hbar\omega_C}{3E} \approx \frac{5}{6}\frac{\gamma {r_E}^2 N_b}{\alpha\sigma_z(\sigma_x + \sigma_y)} \tag{7}$$

where $\alpha \approx 1/137$ is the fine structure constant, and σ_z the rms bunch length. Coherent pair creation becomes the prevailing source of background for Υ above 0.5, a regime avoided in most collider designs.

The number of beamstrahlung photons emitted per electron is

$$N_\gamma \approx \frac{5\alpha\sigma_z}{2\gamma}\,\frac{\Upsilon}{(1+\Upsilon^{2/3})^{1/2}} \approx 2\,\frac{\alpha r_e N_b}{\sigma_x + \sigma_y} \tag{8}$$

where the last approximation applies if Υ is small ($\Upsilon \leq 1$). The number N_γ should not be much larger than 1 for background considerations. The fraction of the luminosity at the design center-of-mass energy is given by $\Delta\mathcal{L}/\mathcal{L} \approx 1/N_\gamma^2(1-e^{-N_\gamma})^2$, and the average relative energy loss due to beamstrahlung is

$$\delta_B \approx \frac{1}{2} N_\gamma \Upsilon = \frac{r_e^3 N_b^2 \gamma}{\sigma_z \sigma_x^2 (1+\sigma_y/\sigma_x)^2} \tag{9}$$

The three quantities Υ, N_γ and δ_B can be reduced by operating with (1) flat beams and (2) long bunches, or by more exotic approaches such as (3) charge compensation (Balakin and Solyak, 1986; Rosenzweig *et al.*, 1989) or (4) a plasma at the interaction point (Whittum *et al.*, 1990).

In terms of N_γ, the luminosity for a flat-beam linear collider may be rewritten as

$$L \approx \left(\frac{10}{r_e}\right) \frac{P_{wall}}{E_{beam}} N_\gamma \frac{1}{\eta \sigma_y} \tag{10}$$

where P_{wall} is the wall plug power, $\eta = P_{beam}/P_{wall}$ the ratio of beam power to wall-plug power (efficiency). If N_γ and the energy are held constant, the luminosity can be raised only by increasing the power-conversion efficiency and by reducing the vertical spot size.

Due to the attraction of the colliding particles by the other beam, the effective beam size at the interaction point is smaller and the luminosity higher by a factor $H_D = \mathcal{L}/\mathcal{L}_{00}$ than it would be without the collision. This so-called pinch effect (Hollebeek, 1981) is significant for disruption parameters $D_{x,y}$ larger than 1.

An empirical formula of the pinch enhancement for head-on round-beam collisions, which was obtained by fitting a large number of simulation results, is (Chen and Yokoya, 1988a):

$$H_D^{round} \approx 1 + D^{1/4} \left(\frac{D^3}{1+D^3}\right) \left\{\ln(\sqrt{D}+1) + 2\ln\left(\frac{0.8}{A}\right)\right\} \tag{11}$$

where $D = D_x = D_y$ and $A = \sigma_z/\beta^\star_{x,y}$. This formula for the factor H_D includes the effect of the depth of focus.

For flat beams, it was both shown in simulations (Chen and Yokoya, 1992) and expected on theoretical grounds (Rosenzweig and Chen, 1991) that

$$H_D^{flat} \approx \left(H_D^{round}\right)^{1/3} \tag{12}$$

where $D = D_y$, $A = A_y$ and $D_x, A_x \approx 0$.

V. CROSSING ANGLE AND CRAB CROSSING

As mentioned, a crossing angle is frequently used to separate the incoming and outgoing beams in a long train of bunches. We will address four primary issues with respect to a crossing angle. The first is simply geometry. The crossing angle needs to be sufficiently large to separate the beams and to provide a passage for the outgoing beam to escape the interaction region. If the crossing-angle is large, it may be possible to have separate quadrupoles for the incoming and outgoing beams while for small crossing angle an exit port is usually needed in the FD quadrupoles.

Second, a multibunch crossing instability (Chen and Yokoya, 1988b) can arise from the parasitic bunch interactions. Assuming flat beams, the criterion to avoid significant vertical displacement of the bunches due to this instability can be expressed as

$$(m_b - 1) \ll \frac{C_\Theta^2}{D_x D_y}\sqrt{\frac{1}{2} + \frac{D_y}{3}} \tag{13}$$

where $D_{x,y}$ are the disruption parameters discussed in Section IV and $C_\Theta = \Theta_c \sigma_z/\sigma_x$ (Θ_c is the trajectory crossing angle); C_Θ is not necessarily the same as C_θ, the bunch crossing angle, which was defined in Section III. In addition, m_b is the number of bunches that interact in the free space around the IP, which, assuming no additional masking, is $m_b = 1 + 2L^\star/\Delta_b$ where Δ_b is the bunch spacing and $L^\star$ is the free distance to the IP. This instability decreases rapidly with larger crossing angles.

Third, if the geometric luminosity loss due to the crossing-angle, Eq. (4), is significant, i.e. when then trajectory crossing-angle Θ_c is large compared to the bunch diagonal angle ($C_\Theta \gtrsim 1$), the beam can be crabbed (Palmer, 1988). Here, the bunches are given a time dependent horizontal position offset so that they collide head-on: $dx^\star/dz = \Theta_c/2$. There are two approaches to establish the crabbing: either use an rf deflecting cavity or use the

correlated energy spread along the bunch and a small amount of residual dispersion at the IP (Brinkmann, 1993). In the latter approach, the required IP dispersion is:

$$\eta_x^\star \frac{\sigma_{\epsilon_c}}{\sigma_z} = \Theta_c/2 \ , \tag{14}$$

where σ_{ϵ_c} is the correlated component of the rms energy spread, while the required rf voltage is

$$V_{rf} = \frac{\Theta_c E \lambda_{rf}}{4\pi R_{12}} \ , \tag{15}$$

where E is the beam energy and R_{12} is the transport matrix element from the crab cavity to the IP. With a fully crabbed beam, the beam crossing-angle θ_c is zero even though the trajectories intersect at an angle.

In general, the tolerances on the alignment and stability of the crab cavity are relatively loose. The exception is the relative phase tolerance between the crab cavities on either side of the IP. A phase difference between the cavities will cause a horizontal offset between the beams. To limit the luminosity dilution to 2%, the bunch separation must be less than $0.3\sigma_x$ rms. This imposes an rms tolerance on the phase difference between the cavities of

$$\Delta\phi_{rf} = 2\pi \frac{0.6\sigma_x}{\Theta_c \lambda_{rf}} \ \text{[radians]} \ . \tag{16}$$

Note that the tolerance on the bunch timing is much looser and just shifts the longitudinal IP position with a luminosity loss that depends on the depth of focus.

Fourth, with a crossing angle, the beams do not travel parallel to the axis of the solenoidal field. For a horizontal crossing angle, this results in vertical deflections of the beams and, perhaps more importantly, in vertical dispersion at the IP. To estimate the effect, we will assume that the FD quadrupoles are outside of the solenoidal field. In this case, the vertical offset at the IP is:

$$\Delta y^\star = \frac{B_s L^{\star 2}}{B\rho} \frac{\Theta_c}{4} \tag{17}$$

where B_s is the solenoidal field and $B\rho$ is a function of the beam energy: $B\rho = 33.356\,\text{E[GeV]}$ (kG-m). This deflection can be corrected by steering but it is more difficult to correct the dispersion introduced by the deflection.

VI. OPTICAL ABERRATIONS

Almost all the aberrations in a FFS arise from the need to correct the chromaticity introduced by the final doublet:

$$\xi_y^\star \equiv \frac{L_y^c}{\beta_y^\star} = -\int ds K_1 \beta_y \approx -\frac{1}{\beta_y^\star}\int ds K_1 R_{34}^2 \tag{18}$$

where K_1 is the normalized quadrupole strength in units of m^{-2}, R_{34} is the $(3,4)$ transport matrix element from position s to the IP, and the approximate relation is valid because the final doublet is $\sim 90^\circ$ from the IP. The quantity L_y^c is the vertical chromatic length which, for an FD where the final quadrupole is vertically focusing, can be limited to be only slightly larger than the free distance from the IP to the first quadrupole, $L^\star$. This is in contrast to the horizontal chromatic length L_x^c which tends to be much larger than $L^\star$ although in a flat beam FFS, where $\beta_x^\star \gg \beta_y^\star$, the horizontal chromaticity is much smaller than the vertical.

If uncorrected, the chromaticity will lead to an energy dependent increase in the spot size:

$$\frac{\Delta\sigma_{x,y}}{\sigma_{x,y}} \approx \xi_{x,y}\sigma_\epsilon \tag{19}$$

to be added in quadrature, where σ_ϵ is the rms energy spread in the beam.

As mentioned, the chromaticity is corrected by placing sextupole magnets, located $n\pi$ in betatron phase from the FD, in regions of dispersion and large beta functions. The total integrated sextupole strength k_2 can be estimated from the need to compensate the FD chromaticity:

$$\text{CCX:}\quad k_2\eta_x\beta_x \approx \xi_x^\star \qquad \text{and} \qquad \text{CCY:}\quad k_2\eta_x\beta_y \approx -\xi_y^\star \tag{20}$$

where we have assumed that the β_y is small in the CCX while the β_x is small in the CCY so that there is little effect of one on the other.

The 3rd-order geometric aberrations due to the sextupoles are canceled by separating the magnets by a $-I$ transformation but there are still other optical aberrations that can

be important. In particular, the chromatic sensitivity of the lattice providing the $-I$ transform between the sextupoles introduces 3rd-order chromaticity and other 4th-order chromo-geometric aberrations (Irwin, 1990). Some of these can be compensated using additional sextupoles placed throughout the final focus (Brinkmann, 1990) or by a non-symmetric dispersion function in the chromatic correction sections (Oide, 1992).

In addition, the finite sextupole length creates octupole-like 4th-order aberrations. For a given sextupole strength and length, the vertical spot size increase due to this aberration is (Roy, 1992):

$$\frac{\Delta\sigma_y^\star}{\sigma_y^\star} = k_2^2 L_s \beta_y^2 \epsilon_y \sqrt{\frac{5}{12} + \frac{\sigma_x^2}{6\sigma_y^2} + \frac{\sigma_x^2}{12\sigma_y^2}} \tag{21}$$

where $\Delta\sigma^\star/\sigma^\star$ is added in quadrature to the unperturbed spot size, the beta functions and beam sizes are evaluated at the sextupole locations, L_s is the sextupole length, and k_2 is the integrated sextupole strength in units of m^{-2}; a similar expression exists for the aberration in the horizontal plane and is found simply by switching the x and y indices.

VII. SYNCHROTRON RADIATION

Synchrotron radiation in the bending magnets that produce the dispersion in the CCX and CCY has two effects: first, it will enlarge the horizontal spot size and divergence (i.e., the horizontal emittance) due to the non-zero dispersion in these locations and, second, the change in the particle energy due to the radiation is not chromatically corrected. The first effect can be estimated (Sands, 1985; Roy, 1992)

$$\Delta\sigma_x^2 = CE^5 \int ds |G^3| \, (R_{16}^{s\to IP})^2 \tag{22}$$

$$\Delta\sigma_{x'}^2 = CE^5 \int ds |G^3| \, (R_{26}^{s\to IP})^2 \tag{23}$$

where $C = 4.13 \times 10^{-11}$ m^2 GeV^{-5}, G is the inverse of the local bending radius, and $R_{i6}^{s\to IP}$ is the (i,6) R-matrix element from location s to the IP ($i = 1, 2$). Note that the FFS can be re-matched to account for the change in the beam phase space orientation, which may result in

a smaller luminosity loss than estimated from the above equations. The rematching usually requires reducing $\beta^\star$ by an amount comparable to the emittance dilution, and is performed emiprically by optimizing the IP beam divergence.

The second effect can be estimated using the chromaticity of the FD:

$$\frac{\Delta\sigma_{x,y}}{\sigma_{x,y}} \approx \Delta\sigma_\epsilon \Delta\xi_{x,y} \tag{24}$$

where $\Delta\xi$ is the uncorrected chromaticity, which is nominally zero upstream of the chromatic correction sections and is equal to $\xi^\star$ downstream of the chromatic correction sections. In addition, σ_ϵ is the rms energy spread which can be expressed

$$(\Delta\sigma_\epsilon)^2 = CE^5 \int ds|G^3| \tag{25}$$

with all quantities defined above.

Another effect due to the synchrotron radiation, referred to as the Oide Effect, arises in the final lens when the radiation changes the particle's energy and this interacts with the local chromaticity (Oide, 1988). The effect depends on fields seen by the beam in the final quadrupoles which is a function of both the horizontal and vertical extent of the beam. In the original reference, the horizontal beam size was ignored and the change in the rms spot size was found to be

$$(\Delta y^\star)^2 = \frac{55 r_e \lambda_e \gamma^5 \sigma_{y'}^{\star\,5}}{3\pi\sqrt{6\pi}} \int ds L_y^{c\,2} R_{34}^3 |K_1|^3 \tag{26}$$

where L_y^c is the chromatic length, defined in Eq. 18.

An approximate expression can be found including the horizontal beam size (Irwin, 1996):

$$\begin{aligned}(\Delta y^\star)^2 \approx\ & 1.22 r_e \lambda_e \gamma^5 \sigma_{y'}^{\star\,2} \times \\ & \int ds L_y^{c\,2} |K_1|^3 (7\sigma_{y'}^{\star\,2} R_{34}^2 + \sigma_{x'}^{\star\,2} R_{12}^2) \sqrt{\sigma_{y'}^{\star\,2} R_{34}^2 + \sigma_{x'}^{\star\,2} R_{12}^2}\ ,\end{aligned} \tag{27}$$

however, the additional contribution from σ_x can be made relatively small by decreasing the strength of the horizontally focusing magnet in the FD.

Finally, it is important to note that even though the rms increase of the spot size due to the Oide effect can be significant, the probability of radiating photons in the FD is rather

small and thus the resulting beam has an unperturbed core with large tails (Hirata *et al.*, 1989). Thus, the actual luminosity decrease is much less than that naively calculated from the above expressions; for details refer to Ref. (Hirata *et al.*, 1989).

VIII. WAKEFIELDS

Wakefields can potentially be dangerous in the FFS because the beta functions are large which makes the beam sensitive to the transverse deflections. In addition, the FD chromaticity is large which makes the beam very sensitive to any longitudinal wakefields between the CCY and the FD; an estimate of the tolerance on the induced energy spread can be made using Eq. (18). Both problems can be compounded by the need for collimators and protection masks which are sometimes placed close to the beam. Thus, when designing a FFS, care must be taken to verify the wakefields of the components in the beam line; examples of such analyses for the SLC and NLC FFS can be found in Refs. (Zimmermann *et al.*, 1996) and (Raubenheimer and Zimmermann, 1996).

In addition to wakefields from the collimators and upstream elements, there are transverse geometric and resistive wakefields that can be important in the final doublet and in the chromatic correction sections, where the beta functions are very large. These wakefields will have two effects: they will increase the beam emittance and they will amplify any centroid jitter; we will discuss the centroid jitter since it imposes the a more restrictive constraint. The centroid jitter amplification due to the resistive wall wakefield is

$$\frac{\Delta y^\star}{\sigma_y^\star} = 1.6 \frac{N r_e}{\gamma \sigma_z} \frac{L \beta_{FD} \delta_s}{g^3} \left(\frac{\Delta y}{\sigma_y} \right)_{FD} \tag{28}$$

where L is the length of the aperture, g is the beam-pipe radius, β_{FD} is the beta function in the final doublet, and $\delta_s = \sqrt{\sigma_z / Z_0 \sigma}$ is the skin depth of the beam pipe.

Similarly, the effect of a gentle taper can be estimated as (Yokoya, 1988)

$$\frac{\Delta y^\star}{\sigma_y^\star} = 0.56 \frac{N r_e}{\gamma \sigma_z} \frac{L \Theta^2 \beta_{FD}}{g_1 g_2} \left(\frac{\Delta y}{\sigma_y} \right)_{FD} \tag{29}$$

where L and Θ are the length and angle of the taper and g_1 and g_2 are the initial and final beam-pipe radii. Fortunately, both of these tolerances depend strongly on the beam pipe radius and thus the effect can be minimized easily.

IX. SCATTERING

There are three scattering processes that are important in a FFS: inelastic (bremsstrahlung) and elastic scattering on the residual gas atoms and scattering on the thermal photons. The cross-section for bremsstrahlung at high energies (assuming complete screening) is (Bethe and Ashkin, 1953)

$$\sigma_{brem} \approx \frac{16}{3}\alpha Z(Z+1.35)r_e^2 \ln\left(\frac{183}{Z^{1/3}}\right)\left[\ln\left(\frac{\delta_{max}}{\delta_{min}}\right) + \delta_{min} - \delta_{max}\right] \tag{30}$$

where α is the fine structure constant, δ_{min} and δ_{max} are the minimum and maximum photon energy in units of the beam energy, and the factor $Z(Z+1.35)$ accounts for the nuclear charge and approximates the atomic electrons; a typical cross-section for CO with large energy losses is a few barns.

Now, the number of scattered beam particles is:

$$\frac{\Delta N}{N} = n_{gas} L \sigma_{brem} \tag{31}$$

where L is the distance the beam travels, $n_{gas} = 3.2 \times 10^{22} P N_{atom}\,\mathrm{m}^{-3}\,\mathrm{Torr}^{-1}$ at 300° K, P is the vacuum pressure, and N_{atom} is the number of atoms per molecule of gas.

A similar effect arises from the inverse-Compton scattering with thermal photons (Telnov, 1987). The scattering can be described with the parameter

$$x \equiv \frac{4E\omega\hbar}{m_e^2 c^4}\sin^2(\theta/2) \tag{32}$$

where E and $\hbar\omega$ are the beam and photon energies and the θ is the angle between the photon and the beam. The maximum energy of the scattered photon is

$$\hbar\omega'_{max} = \frac{x}{1+x}E \tag{33}$$

and, because the beam energy is much higher than the photon energy, a large fraction of the scattered photons are close to this maximum energy.

Now, the photon density is described by the Plank blackbody formula

$$\frac{dn}{d\omega} = \frac{\omega^2}{\pi^2 c^3 (e^{\hbar\omega/kT} - 1)} \tag{34}$$

with a total number of photons and an average photon energy of

$$n = 2 \times 10^7 T^3 \, [^\circ\mathrm{K}^{-3}\mathrm{m}^{-3}] \qquad \text{and} \qquad \hbar\omega_{ave} = 2.7kT \; . \tag{35}$$

Unfortunately, to calculate the number of large amplitude scatterings, the differential cross-section needs to be integrated over θ and the photon density function which must be done numerically. This and other scattering processes in the final focus can be studied with Monte-Carlo simulations (Reichel *et al.*, 1998).

The effect can roughly be estimated by assuming that half the photons are scattered to the maximum energy, calculated from the average photon energy, and then multiplying the total photon density with the total Compton cross-section, i.e.

$$\frac{\Delta N}{N} = 0.5 n L \sigma_c \tag{36}$$

where

$$\frac{\Delta E}{E} = \frac{x_{ave}}{1 + x_{ave}} \qquad \text{and} \qquad x_{ave} = \frac{10.8 E k T}{m_e^2 c^4} \tag{37}$$

and the total Compton cross-section is:

$$\sigma_c = \frac{2\pi r_e^2}{x_{ave}} \left[\left(1 - \frac{4}{x_{ave}} - \frac{8}{x_{ave}^2} \right) \ln(1 + x_{ave}) + \frac{1}{2} + \frac{8}{x_{ave}} - \frac{1}{2(1 + x_{ave})^2} \right] \; . \tag{38}$$

For typical parameters, this expression tends to over-estimate the number of large amplitude scatterings by a factor of 2–5.

Finally, we can calculate the effect of elastic Coulomb collisions. Here, the incident particles can scatter off the nucleus or the atomic electrons. In the former case, the energy change of the incident particle is relatively small and the primary effect is an angular deflection that

may cause the particle to exceed the beam-pipe aperture. In comparison, the energy change can be significant when scattering off the atomic electrons.

The differential cross-section for Coulomb scattering on atomic nuclei can be written:

$$\frac{d\sigma_{en}}{d\Omega} = \frac{4F^2(q)Z^2r_e^2}{\gamma^2}\frac{1}{(\theta^2+\theta_{min}^2)^2} \tag{39}$$

where θ_{min} is a function of the screening due to the atomic electrons and is $\theta_{min} \approx \hbar/pa$ where p is the incident particle momentum and a is the atomic radius: $a \approx 0.22\lambda_e/\alpha Z^{1/3}$. In addition, $F(q)$ is the nuclear form factor which for relatively small scattering angles can be approximated by 1 and we have neglected the recoil of the nucleus; both of these later effects will reduce the large angle scattering and will cause us to slightly over-estimate the particle loss.

Now, assuming that the aperture is limited at a single location, such as the final doublet, the number of particles scattered to an amplitude greater than the aperture is:

$$\frac{\Delta N}{N} = n_{gas}L\frac{2\pi Z^2r_e^2}{\gamma^2 b^2}\int ds(R_{12}^2+R_{34}^2) \tag{40}$$

where b is the limiting radius, R_{12} and R_{34} are the transfer matrix elements from the scattering position to the aperture, and we have assumed that $b^2 \gg (R_{12}^2+R_{34}^2)\theta_{min}^2$.

Next, we can calculate the elastic scattering with the atomic electrons. Here, the angular deflection can be accounted for by replacing Z^2 with $Z(Z+1)$ in Eq. (40); this will over-estimate the scattering but is a small correction anyway. However, as mentioned, in this case, the recoil of the electron cannot be neglected and can result in a significant energy change to the incident particle. The differential cross-section for a relative energy change of δ is:

$$\frac{d\sigma_{ee}}{d\delta} = \frac{2\pi Zr_e^2}{\gamma}\frac{1}{\delta^2} \tag{41}$$

and the number of particles scattered beyond a limiting energy aperture δ_{min} is:

$$\frac{\Delta N}{N} = n_{gas}L\frac{2\pi Zr_e^2}{\gamma}\frac{1}{\delta_{min}}\ . \tag{42}$$

X. TOLERANCES

In this section, we will discuss tolerances on the elements in the FFS. However, we should note that it is impossible to separate the tolerances from the tuning procedures (briefly discussed in the next section). For example, to calculate the amount of dispersion generated by moving a quadrupole, one also has to know where the resulting trajectory oscillation is corrected. In the following, we will neglect the tuning and simply calculate "bare" tolerances but it should be emphasized that these are frequently unrealistically tight. To further simplify the discussion, we will only consider effects that contribute to the vertical spot size since these tolerances are usually significantly more stringent than those in the horizontal plane. Finally, we will only discuss the effects or sensitivities of the elements; the final design tolerances must be determined so as to limit the total dilution and require balancing the difficulty with the sensitivities.

A. Incoming Beam

If the geometric aberrations in the FFS are well corrected, the nonlinear aberrations will not be very sensitive to incoming betatron oscillations or changes in the incoming beam emittance. The $-I$ transformations in the CCX and CCY will cause most aberrations to cancel. However, synchrotron radiation in the quadrupoles, and especially the final doublet (Section VII), can impose severe constraints on the incoming trajectory jitter.

B. Trajectory Errors

The dominant source of vertical trajectory errors are movements of the quadrupoles and rolls of the bending magnets. The position at the IP is simply given by the R_{34} transport matrix element from the element to the IP times the deflecting angle:

$$\Delta y^\star = y_q \int ds K_1 R_{34} \qquad \text{and} \qquad \Delta y^\star = \theta_b \int ds G R_{34} \tag{43}$$

where y_q and θ_b are the quadrupole offset and the bending magnet roll.

Assuming the optical functions vary slowly along the magnet, these expressions can be written in the simpler form:

$$\frac{\Delta y^\star}{\sigma_y^\star} = y_q k_1 \sqrt{\frac{\beta_y}{\epsilon_y}} |\sin(\psi_y^\star - \psi_y)| \tag{44}$$

and

$$\frac{\Delta y^\star}{\sigma_y^\star} = \theta_b \Theta_b \sqrt{\frac{\beta_y}{\epsilon_y}} |\sin(\psi_y^\star - \psi_y)| \tag{45}$$

where Θ_b is the bending angle of the bending magnet, β_y is evaluated at the magnet, and, for most magnets in the FFS, $|\sin(\psi_y^\star - \psi_y)| \approx 1$. In the subsequent sections, we will present the sensitivities in terms of the transport matrix elements which is convenient for calculations but it is straightforward to transform them into this more intuitive form.

The tightest quadrupole sensitivity is almost always that on the final doublet, where assuming that the doublet moves as a unit, the trajectory motion at the IP is roughly equal to the motion of the magnets. The sensitivity is even tighter for an asymmetric motion where the horizontally and vertically focusing final magnets move in opposite directions. Fortunately, most of the motion of the magnets in the FFS will be driven by ground motion which tends to be correlated over long distances. In this case, the sensitivities are greatly relaxed because the deflections cancel naturally (Juravlev em et al., 1993; Zhuravlev *et al.*, 1995; Irwin *et al.*, 1996).

C. Dispersion

In the same manner as for the trajectory, we can estimate the dispersion generated by deflections. Here, two effects contribute, the chromatic dependence of the deflection and the chromatic dependence of the displaced downstream trajectory:

$$\Delta\sigma_y^\star = y_q k_1 \sigma_\epsilon |R_{34} - T_{346}| \qquad \text{and} \qquad \Delta\sigma_y^\star = \theta_b \Theta_b \sigma_\epsilon |R_{34} - T_{346}| \ , \tag{46}$$

where σ_ϵ is the rms energy spread and T_{346} is the 2nd-order transport element which will dominate downstream of the CCY because of the uncorrected vertical chromaticity.

Vertical dispersion can also be generated by rolls of the quadrupole magnets or displacements of the sextupole magnets:

$$\Delta\sigma_y^\star = 2\theta_q\eta_x k_1\sigma_\epsilon|R_{34}| \qquad \text{and} \qquad \Delta\sigma_y^\star = y_s\eta_x k_2\sigma_\epsilon|R_{34}| \tag{47}$$

where η_x is the horizontal dispersion evaluated at the magnet and θ_q and y_s are the roll of the quadrupole and offset of the sextupole magnets.

D. Skew Coupling

Skew coupling is generated by direct skew fields or by trajectory errors that cause offsets in the sextupoles. The direct skew fields arise from the detector solenoid as well as rolls of the quadrupole magnets or displacements of the sextupole magnets. In this case,

$$\Delta\sigma_y^\star = 2\theta_q k_1\sigma_x|R_{34}| \qquad \text{and} \qquad \Delta\sigma_y^\star = y_s k_2\sigma_x|R_{34}| \tag{48}$$

where σ_x is the horizontal beam size at the magnet; the tightest roll tolerances are usually found for the FD magnets. Of course, the FFS must be designed with tuning elements to correct for the skew coupling since it is part of the design optics and is introduced by the detector solenoid. Fortunately, with flat beams, the skew correction only needs to be applied to the two phases that enlarge the vertical beam size at the IP, i.e. the $x^\star$-$y^\star$ and $x'^\star$-$y^\star$ terms, since the sensitivities for the horizontal beam size are much looser.

Another source of coupling are trajectory errors that displace the beam in one of the paired sextupoles of the CCX or CCY; because the sextupoles are separated by a $-I$ transformation, an oscillation passing through both magnets will have little effect but an offset in one of the magnets can have a large effect. Hence, this introduces additional sensitivities for the magnets inside the CCX or CCY:

$$\Delta\sigma_y^\star = \theta_b\Theta_b|R_{34\,b\to s}|k_2\sigma_x|R_{34\,s\to\star}| \tag{49}$$

and

$$\Delta\sigma_y^\star = y_q k_1 |R_{34\,q\to s}| k_2 \sigma_x |R_{34\,s\to\star}| \tag{50}$$

where $R_{34\,b\to s}$ and $R_{34\,s\to\star}$ are the transport matrix elements from the bending magnet to the sextupole where the trajectory is offset and then from the sextupole to the IP. Because of the strong focusing in the CCX and CCY, small errors can result in large trajectory offsets at the sextupoles and this can be one of the more severe sensitivities.

XI. TUNING

In the FFS most important high-order aberrations are minimized by design and the tolerances on the accuracy of their cancellations are relatively loose. However, the tolerances on the low-order aberrations are much tighter and thus tuning strategies must be developed to minimize these aberrations routinely. For example, it is thought that in the NLC FFS (Zeroth Order Design Report, 1996; Zimmermann *et al.*, 1997), the 1st-order aberrations, such as dispersion and IP waist position, will probably need to be tuned on an hourly basis, while the 2rd-order and 3rd-order aberrations, such as chromaticity and 2nd-order dispersion, will need weekly to monthly tuning, and the 4th-order aberrations are neglected.

To prevent luminosity loss, the tuning procedures must be designed to use orthogonal corrections for fast convergence to the optimal solutions (Walker *et al.*, 1993). Simulation tools have been found very effective for testing the procedures at the SLC (Woodley, 1994) and more recently the MERLIN code (Walker, 1997) has been developed as part of the TESLA project.

Finally, the tuning procedures, which are usually based on beam size measurements, are very sensitive to the accuracy of the measurements. It is presently thought that imperfect spot size measurements during the tuning of the low-order aberrations in the SLC was causing a 20 to 30% luminosity loss until the 1997 SLC run (Emma *et al.*, 1997). Thus, very accurate diagnostics are essential for the FFS. To alleviate this problem, the SLC FFS is now

being tuned using dither feedback systems based on measurements of the energy loss due to beamstrahlung as described in Ref. (Emma *et al.*, 1997) with roughly an order-of-magnitude improvement in the tuning efficiency (Hendrickson em et al., 1997).

XII. OPTIMIZATION

The aberrations in a final-focus system as well as the effect of errors on the spot size can be analyzed using Lie-algebra techniques (Roy, 1992; Irwin, 1990), advanced software tools which combine Lie algebra with truncated-power series algebra and particle tracking, for example the programs DESPOT (Forest, 1997) or LEGO (Cai *et al.*, 1997), or more conventional element-to-element multi-particle tracking codes such as TURTLE (Brown and Iselin, 1974) or DIMAD (Servranckx, 1990). DIMAD includes the effect of synchrotron radiation in bending magnets and quadrupoles (Roy, 1990). Specific automatic design and analysis programs for generic final-focus systems have also been developed, for example, the codes FFADA (Dunham and Napoly, 1994) and LCOPT (Yokoya, 1997).

XIII. ADVANCED DEVELOPMENTS

Several novel techniques have been proposed to overcome some of the design limitations of 'conventional' FFS. One important characteristic of a final-focus system is its momentum bandwidth. In most present generation FFS, using separate CCX and CCY sections, the bandwidth is typically limited by the chromatic breakdown of the $-I$ transform between sextupole pairs. This gives rise to fifth-order chromatic and chromo-geometric terms such as described by the Lie generators $p_x p_y^2 \delta^2$ and $p_y^2 \delta^3$. The bandwidth can be improved by introducing additional sextupoles (Brinkmann, 1990) in the final transformer and in the chromatic correction section and/or by an odd-dispersion optics, where the dispersion at the first sextupole is zero or of opposite sign to the second sextupole (Oide, 1992). While the odd-dispersion optics minimizes the term $p_x p_y^2 \delta^2$ (Oide, 1992), the additional sextupoles can also be employed to reduce the third-order chromaticity (generator $p_y^2 \delta^3$) (Zeroth Order

Design Report, 1996). Most of the fifth-order aberrations decrease with increasing value of dispersion at the sextupoles.

Another technique, referred to as a traveling focus (Balakin, 1992), might be used to avoid the luminosity reduction due to the depth of focus (Eq. (4)), which can be significant when $\sigma_z \geq \beta^*$. Here, the optical focal point is varied depending on the longitudinal position within the bunch. Particles in the head are focused at the actual interaction point. As the collision progresses, the focal points of both beams are shifted gradually backwards in longitudinal position, such that particles in the later parts of the bunches are focused at a point where they first come into contact with the opposing beam. The ensuing pinch effect then sustains a small spot size throughout the entire collision process. A traveling focus can be implemented either using uncorrected chromaticity and an energy-position correlation across the bunch or with a fast rf quadrupole.

Another problem is the length of a conventional FFS, which already at a beam energy of 0.5 TeV can occupy a significant fraction of the collider. In scaling to higher energies, the FFS length would increase quadratically with the energy (Zimmermann *et al.*, 1995). This quadratic scaling assumes that (1) the luminosity should grow as the square of the energy, (2) the normalized emittances and the free length from the IP are held constant, and (3) the total length of the final-focus system is determined by synchrotron radiation in the bending magnets and by magnet position tolerances. Different assumptions could imply a slightly weaker growth ($\sim \gamma^{3/2}$) (Irwin, 1997), however, the length still increases rapidly with the beam energy.

The final-focus length is determined to a large extent by its natural chromaticity which in turn depends on the strength of the final quadrupoles and their proximity to the interaction point. Strong lenses very close to the IP would allow a significant reduction of the system length. Plasma lenses have been suggested as one tool to provide strong focusing near the IP. If a plasma is placed just in front of the interaction point, the beta function at the IP is reduced to (Chen *et al.*, 1996; Chen *et al.*, 1993)

$$\frac{\beta^*_{x,y}}{\beta^*_{0,x,y}} = \frac{1}{1 + K\beta^*_{0,x,y}\bar{\beta}_{x,y}} \tag{51}$$

where $K \approx 2\pi r_e n_p/\gamma$ (n_p is the plasma density) denotes the quadrupole gradient of the plasma lens, $\beta^*_{0,x,y}$ the horizontal (vertical) IP beta function without the plasma lens, and $\bar{\beta}_{x,y}$ the beta function at the entrance to the lens of thickness d:

$$\bar{\beta}_{x,y} = \beta^*_{0,x,y}\left(1 + \left(\frac{d}{\beta^*_{0,x,y}}\right)^2\right) \tag{52}$$

Unfortunately, this technique works best for electron beams. Positron beams responds very differently to a plasma lens and, although it is not impossible to also focus a positron beam with a plasma, such focusing will introduce strong optical aberrations (Chen *et al.*, 1989).

If the plasma-density gradient is properly chosen, one can realize an adiabatic focusing lens which can bypass the Oide limit on the vertical spot size (Chen *et al.*, 1990). A new limit on the spot size arises from energy-loss considerations:

$$\sigma_q \gg (1.39 \times 10^{-8}\ \text{m}\ )\ \xi^2 \exp\left(-\frac{1.12}{\xi}\right) \tag{53}$$

where $\xi = (\gamma\epsilon_y/\epsilon_c)^{1/3}$ with $\epsilon_c \approx 6.2\ \mu$m.

Similarly, it may be possible to use the intense fields of demagnified low-energy bunches as a final lens. Here, the primary bunches collide with low energy oppositely-charged bunches a short distance from the IP. Also in this technique, referred to as 'dynamic focusing', the final lens, i.e. the low-energy bunches, is located close to the IP and thus the FFS chromaticity can be quite small. However, the pinch effect in the focusing collision would cause a luminosity loss (Irwin, 1997)

$$\frac{\Delta L}{L} \approx \frac{2}{15}\ \left(\frac{f_M \sigma_z}{f_Q \beta^*_M}\right)^2 \tag{54}$$

where $f_M = l^*$ is the focal length for the main beam, and f_Q the focal length of the lens beam, and β^* the IP beta function including the focusing effect from the lens beam. A rather short main-beam bunch length σ_z is required to avoid this luminosity loss.

Finally, a different approach, attractive for very high energy colliders, is to completely abandon the chromatic correction and to build a compact final focus consisting only of a

few quadrupole lenses. This saves the space otherwise needed for the bending magnets, and thus, considerably shortens the FFS. In addition, the tight tolerances on the relative alignment of beam orbit and sextupoles are eliminated. The disadvantage is that the absence of chromatic correction requires a very small incoming energy spread (Zimmermann and Whittum, 1997; Zimmermann, 1998).

ACKNOWLEDGEMENTS

Many people have contributed to the advancements in linear-collider final-focus systems and to the present design philosphy. We had the pleasure to work with some of them, and would like to thank, in particular, R. Brinkmann, K. Brown, P. Chen, P. Emma, R. Helm, J. Irwin, O. Napoly, K. Oide, N. Walker, D. Whittum and K. Yokoya for sharing their insights and for inspiring discussions.

REFERENCES

Balakin, V.E., and N.A. Solyak, Proc. XIII Intern. Conf. on High Energy Accelerators, Novosibirsk, USSR (1986).

Balakin, V., 1992, Proc. of the Int. Work. on FF and Int. Regions, SLAC–405.

Bethe, H., J. Ashkin, 1953, "Passage of Radiations through Matter," Experimental Nuclear Physics, Vol. 1, edited: E. Segre, Wiley, New York (1953).

Brinkmann, R., "Optimization of a Final Focus System for Large Momentum Bandwidth," DESY–M–90/14 (1990).

Brinkmann, R., 1993, Proc. Fifth Int. Work. Next-Generation Linear Colliders, Stanford, CA, SLAC–436.

Brown, K.L., and F.C. Iselin, 1974, "DECAY TURTLE (Trace Unlinited Rays Through Lumped Elements): A Computer Program for Simulating Charged Particle Beam Transport Systems, Including Decay Calculations", CERN–74–2.

Brown, K.L., J. Spencer, 1981, 1981 Part. Accel. Conf., Washington D.C., 2568.

Cai, Y., *et al.*,, "LEGO: A Modular AcceleratorDesign Code," Proc. of 17th IEEE Particle Accelerator Conference (PAC 97), Vancouver, Canada, 12-16 May (1997).

Chen, P., and K. Yokoya, 1988, Physical Review D, **38**, no. 3.

Chen, P., and K. Yokoya, 1988, "Multibunch Crossing Instability," SLAC–PUB–4653.

Chen, P., S. Rajagopalan, J. Rosenzweig, 1989, Phys. Rev. D 40, 923 (1989).

Chen, P., K. Oide, A.M. Sessler, and S.S. Yu, 1990, Part. Acc. **31**, 7.

Chen, P., and K. Yokoya, 1992, in 'Frontiers of Particle Beams: Intensity Limitations', Lecture Notes in Physics 400, Springer-Verlag.

Chen, P., C.K. Ng and S. Rajagopalan, Physical Review E 48, no. 4, 3022 (1993).

Chen, P., A. Spitkovsky and A. Weidemann, 1996, Int. Journ. of Mod. Phys. A, Vol. 11, no. 9, 1687 (1996).

Conceptual Design of a 500 GeV e^+e^- Linear Collider with Integrated X-ray Laser Facility, 1997, DESY 1997–048.

Dunham, B., O. Napoly, 1994, "FFADA, Final Focus Automatic Design and Analysis," DAPNIA/SEA 94-06.

Emma, P., *et. al.,* "Limitations of Interaction-point Spot-size Tuning at the SLC," Proc. 1997 Part. Acc. Conf., Vancouver, CN (1997).

Final Focus Test Beam: Project Design Report, 1991, SLAC–376.

Forest, E., unpublished (1997).

Hendrickson, L., *et al.*, 1997, "Luminosity Optimization Feedback in the SLC," Proc. of ICALEPCS 1997.

Hollebeek, R., 1981, Nucl. Instr. Meth. **184**, 333.

K. Hirata, B. Zotter, K. Oide, 1989, Phys. Let. B **224** 437.

International Linear Collider Technical Review Committee Report, G.A. Loew ed., SLAC–R–95–471 (1995) with updates available at: http://www.slac.stanford.edu/xorg/ilc-trc/ilc-trchome.html.

Irwin, J., Nucl. Instr. Meth. A **298**, 460.

Irwin, J., Eq. (11.111) in Ref. (Zeroth Order Design Report, 1996).

Irwin, J., *et. al.,* "Ground Motion: Theory and Measurement," Appendix C of Ref. (Zeroth Order Design Report, 1996).

Irwin, J., "Dynamic Focusing Schemes for Linear Colliders," 1997 IEEE Part. Acc. Conf., Vancouver, Canada (1997).

JLC Design Study, 1997, KEK–REPORT 97–1.

Juravlev, V.M., *et. al.*, 1993, "Investigations of Power and Spatial Correlation Characteristics of Seismic Vibrations in the CERN LEP Tunnel for Linear Collider Studies," CERN-SL-93-53.

Myers, S., 1995, Proc. IEEE Part. Acc. Conf., Dallas, Texas, 476.

Murray, J.J., K.L. Brown, T. Fieguth, 1987, 1987 Part. Accel. Conf., Washington D.C., 1331.

Oide, K., 1988, Phys. Rev. Let., **61** 1713.

Oide, K., 1992, Proc. 15th High Energy Acc. Conf., Hamburg, Germany, 861.

Palmer, R., 1988 in Snowmass DPF Summer Study 1988: High Energy Physics in the 1990's, Snowmass, Colorado, 613.

Raubenheimer, T., F. Zimmermann, 1996, NLC–Note–23.

Reichel, I., *et al.*, 1998, Proc. of the 1998 International Computational Accelerator Physics Conference (ICAP'98), Monterey, to be published.

Rosenzweig, J.B., B. Autin and P. Chen, 1989, Proc. of the 1989 Lake Arrowhead Workshop on Advanced Accelerator Concepts, AIP, 324.

Rosenzweig, J.B., and P. Chen, 1991, 1991 Part. Accel. Conf., San Francisco, (1991).

Roy, G., 1990, Nucl. Instrum. Meth. A **298**, 128.

Roy, G., "Analysis of the Optics of the Final Focus Test Beam using Lie Algebra Based Techniques," 1992, PhD Thesis, SLAC–397.

Sands, M.,"Emittance Growth from Radiation Fluctuations," SLAC AP–47.

Seeman, J., 1990, Ann. Rev. Nucl. Part. Sci. **41**, 389.

Servranckx, R., *et al.*,, 1990, "User's Guide to the Program DIMAD," SLAC-0285.

Telnov, V., 1987, Nucl. Instr. Meth. A **260**, 304.

Walker, N., *et. al.,* "Global Tuning Knobs for the SLC Final Focus," 1993 Part. Accel. Conf., Washington D.C. (1993).

Walker, N., 1997, "Merlin", presented at Linear Collider 97 workshop, Dubna, Russia.

Whittum, D.H., A.M. Sessler, J.J. Stewart and S.S. Yu, 1990, Part. Acc., **34**, 89.

Woodley, M., 1994, private communication.

Yokoya, K., 1988, "Impedance of Slowly Tapered Structures," CERN SL/90-88.

Yokoya, K., 1997, private communication.

Zeroth-Order Design Report for the Next Linear Collider, 1996, LBNL–PUB–5424, SLAC–474, UCRL–ID–124161.

Zhuravlev, V.M., *et. al.*, 1995, "Seismic Conditions in Finland and Stability Requirements for the Future Linear Collider," HU-SEFT-R-1995-01.

Zimmermann, F., R. Helm, J. Irwin, "Optimization of the NLC Final Focus System," Proc. 1995 Part. Acc. Conf., Dallas, TX (1995).

Zimmermann, F., *et. al.*, 1996, "Collimator Wake Fields in the SLC Final Focus," Proc. Europ. Part. Acc. Conf., Sitges, Spain, 504.

Zimmermann, F., *et. al.*, 1997, "Performance Issues, Downtime Recovery and Tuning in the Next Linear Collider (NLC)," Proc. 1997 Part. Acc. Conf., Vancouver.

Zimmermann F., and D.H. Whittum, 1997, Proc. of the 2nd International Workshop on Electron-Electron Interactions at TeV Energies, Santa Cruz, California, 1997, Int. J. of Modern Physics A, Vol. 13, no. 14, June 1998, p. 2525.

Zimmermann F., 1998, Proc. of 8th Workshop on Advanced Accelerator Concepts, Balti-

more, Maryland.

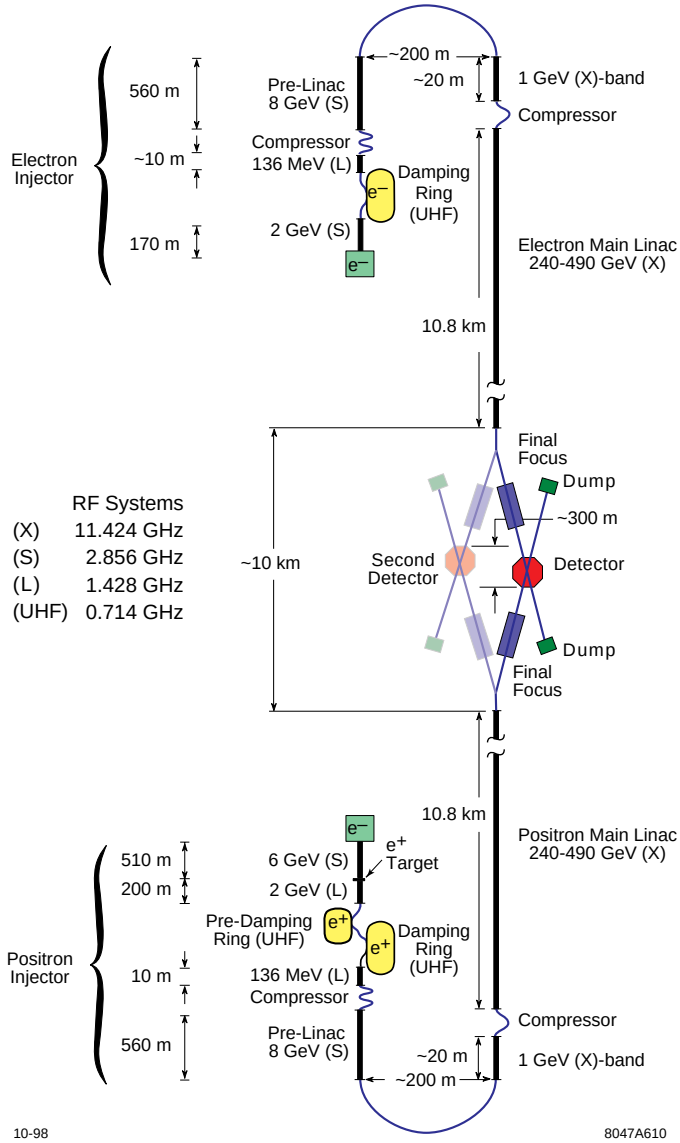

FIG. 1. Schematic of the Stanford NLC, a future 1-TeV linear collider.

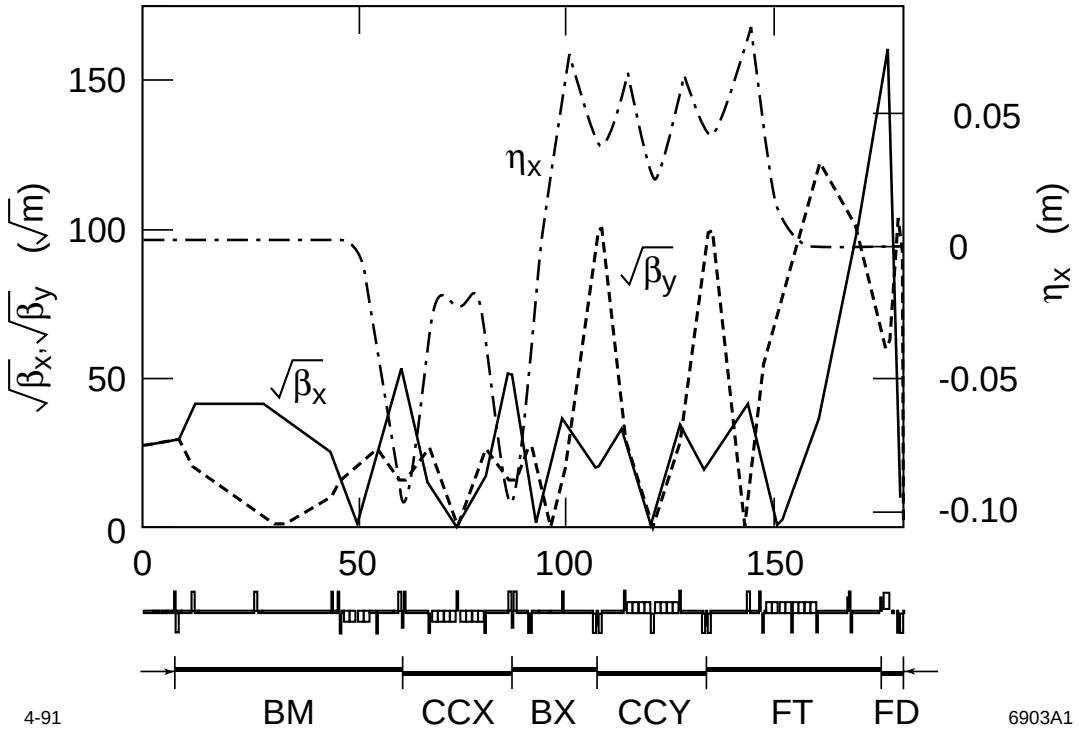

FIG. 2. Schematic of the FFS of the FFTB; from Ref. (FFTB Design Report, 1991).